



Conditions for super-adiabatic droplet growth after entrainment mixing

Fan Yang¹, Raymond Shaw¹, and Huiwen Xue²

¹Atmospheric Sciences Program and Department of Physics, Michigan Technological University, Houghton, Michigan

²Department of Atmospheric and Oceanic Sciences, School of Physics, Peking University, Beijing, China

Correspondence to: Raymond Shaw (rashaw@mtu.edu)

Abstract. Cloud droplet response to entrainment and mixing between a cloud and its environment is often considered by itself, without accounting for subsequent growth after the mixing event. Here we consider the change in cloud properties when the mixed parcel rises adiabatically after the mixing event. The vertical profile for liquid water mixing ratio after a mixing event is derived analytically, allowing the reduction due to mixing to be predicted from the mixing fraction and the cloud and environment temperature and humidity. It is derived for the limit of homogeneous mixing. The expression leads to a critical height above the mixing level: At the critical height the cloud droplet radius is the same for both mixed and unmixed parcels, and the critical height is independent of the updraft velocity and mixing fraction. Cloud droplets in a mixed parcel are larger than in an unmixed parcel above the critical height, which we refer to as the “super-adiabatic” growth region. Analytical results are confirmed by a bin microphysics cloud model. Using the model, we explore the effects of updraft velocity, aerosol source in the environmental air, and polydisperse cloud droplets. Results show that the mixing parcel is more likely to reach the super-adiabatic growth region when the environmental air is humid and clean. It is also confirmed that the analytical predictions are matched by the volume-mean cloud droplet radius under polydisperse conditions. The findings have implications for the origin of large cloud droplets that may contribute to onset of collision-coalescence in warm clouds.

1 Introduction

Warm clouds play an important role for the water cycle and energy balance in the atmosphere. However their formation, development and precipitation processes, are still not fully understood (e.g., Beard and Ochs III, 1993). Observations show that warm clouds can precipitate within 20 minutes (e.g., Laird et al., 2000; Göke et al., 2007). One open question is how small cloud droplets, which are on the order of 10 μm , change to rain drops, usually larger than 1 mm, within such a short time. Because condensation growth is slow for droplet size larger than approximately 20 μm , collision



25 growth is believed to be the most important mechanism for warm cloud precipitation (Pruppacher
et al., 1998).

However, collision efficiency is very low for droplets smaller than $r \approx 30 \mu\text{m}$ due to hydrody-
namic interaction. For example, Hocking (1959) simulated two moving droplets in the Stokes flow
30 approximation, and found that the collision efficiency for a $r = 19 \mu\text{m}$ droplet with smaller droplets
is mostly less than 0.1, and even for a $r = 30 \mu\text{m}$ droplet it is mostly less than 0.5. Such low collision
efficiency suppresses the time required for drizzle and precipitation formation. Therefore, large cloud
droplets are needed to efficiently initiate precipitation. There are several hypotheses to explain the
formation of large cloud droplets: For example, the stochastic collision process itself may produce
35 a small number of “lucky” droplets with larger growth rates (Kostinski and Shaw, 2005). Another
possible mechanism is due to the giant cloud condensation nuclei. Observational results show that
giant and ultragiant CCNs often exist in the atmosphere, and simulation results indicate that they can
be sufficient to start the rain precipitation (e.g., Johnson, 1982; Feingold et al., 1999; Yin et al., 2000;
Blyth et al., 2003; Jensen and Lee, 2008; Cheng et al., 2009). But in this paper we focus on mech-
40 anisms involving the condensation process. For example, results from Lagrangian tracking studies
suggest that large droplets from condensation growth within parcels having favored trajectories can
trigger collisions and drizzle formation in warm clouds (Lasher-Trapp et al., 2005; Cooper et al.,
2013; Magaritz-Ronen et al., 2015; Naumann and Seifert, 2015; Lozar and Muessle, 2016). Korolev
et al. (2013) proposed that droplet size distribution can be broadened through diffusion growth due
45 to cloud base mixing and vertical fluctuation. Perhaps counter-intuitively, the mixing and entrain-
ment that occurs during cloud evolution itself may be responsible for generating large cloud droplets
(Baker et al., 1980). The possibility that that entrainment and subsequent growth can lead to droplets
larger than would occur in an unmixed parcel has occupied the attention of the cloud physics com-
munity for several decades (e.g., Baker et al., 1980; Jensen et al., 1985; Paluch and Knight, 1986;
50 Cooper et al., 2013; Schmeissner et al., 2015).

Observational results show that the number concentration of cloud droplets at the cloud edge/top
is usually smaller than that in the cloud due to entrainment and mixing with environmental air. How-
ever, the mean size of cloud droplet at the edge/top might be smaller, equal to, or even larger than
55 that in the cloud (e.g., Burnet and Brenguier, 2007; Lehmann et al., 2009; Lu et al., 2013; Beals et al.,
2015), which is thought to be the result of different mixing processes. Baker et al. (1980) proposed
two limiting mixing processes: homogeneous and extreme inhomogeneous mixing. Theoretically,
mean cloud droplet size will decrease for homogeneous mixing, but remains the same for extreme
inhomogeneous mixing. However the actual mixing process near the cloud edge/top and the response
60 of cloud droplets to the mixing process are still unclear. Recently, considerable theoretical and com-
putational work has been directed toward understanding the evolution of the droplet size distribution



during both homogeneous and inhomogeneous mixing processes (Andrejczuk et al., 2009; Kumar et al., 2014; Tölle and Krueger, 2014; Korolev et al., 2015; Pinsky et al., 2015b, a). Most of these analyses, however, did not consider the subsequent vertical movement of the mixed parcel, which is also relevant to the evolution of cloud droplets (Wang and Grabowski, 2009; Yum et al., 2015; Chen et al., 2015). Finally, most theoretical work thus far does not account for the possibility of secondary activation of aerosols after dilution and mixing, although there is compelling experimental evidence that this occurs (Burnet and Brenguier, 2007; Schmeissner et al., 2015).

In this study, we are interested in the change of cloud microphysical properties after isobaric mixing of cloudy and clear-air volumes, assuming the mixing parcel rises adiabatically afterwards. This view of a single mixing event followed by isolated growth is an idealization that allows us to understand the microphysical response in the simplest of conditions. We pose the question, is it possible to achieve “super-adiabatic” droplet diameters as a result of mixing? By super-adiabatic, we mean that the droplet diameter is larger than that observed for an unmixed, closed parcel that grows according to moist-adiabatic conditions (as defined, for example, by Cotton et al. (2011, , Chap. 4)). Specifically, we look for the conditions, such as mixing fraction, ambient humidity, aerosol entrainment, secondary activation, and vertical displacement above the mixing level, that influence the ability to produce larger droplets than exist in an unmixed parcel. We first address the problem by deriving analytical results in Section 2, and then evaluate the theory and explore conditions for super-adiabatic droplet growth using a microphysical cloud parcel model in Section 3. Implications are discussed and results are summarized in Section 4.

2 Analytical results

As in previous studies, we consider the final state of the microphysical variables (e.g., liquid water mixing ratio, droplet sizes) after homogeneous mixing (e.g., Korolev et al., 2015). This corresponds to the limit of instantaneous mixing, under which conservation of energy and mass result in a unique dependence of droplet size on the mixing fraction (e.g., Andrejczuk et al., 2006; Burnet and Brenguier, 2007; Gerber et al., 2008; Kumar et al., 2014). Here, we consider the similar two stages of homogeneous mixing process as discussed in (Pinsky et al., 2015b), except that the cloud parcel has continuous vertical movement after the mixing event. The first stage is (instantaneous) isobaric mixing in the absence of phase transitions, and the second stage is the response of the droplets in a vertically moving adiabatic (i.e., closed) parcel. Analytical results in this section are derived under the following assumptions: 1) only liquid exists in the condensed form (no ice); 2) the cloud parcel rises adiabatically; 3) the droplet size distribution is monodisperse; 4) the growth of droplets is



due to water vapor condensation; 5) sedimentation and collision–coalescence of droplets are ignored.

2.1 Liquid water mixing ratio in an adiabatic cloud without mixing

For reference, we begin by deriving the change of liquid water mixing ratio in a rising adiabatic
 100 cloud parcel without mixing. Considering a warm cloud parcel with monodisperse cloud droplets
 rising adiabatically with a constant updraft velocity, the supersaturation development equation is
 (Lamb and Verlinde, 2011, p. 417)

$$\frac{ds}{dt} = Q_1 w - Q_2 \frac{dq_l}{dt}, \quad (1)$$

where s is supersaturation, w is updraft velocity, and q_l is the liquid water mixing ratio (g kg^{-1}).
 105 Q_1 and Q_2 depend on temperature, pressure and other constants (all symbols and expressions are
 given in the Appendix). The first term on the right side represents the production of supersatu-
 ration due to adiabatic cooling due to vertical displacement, while the second term accounts for
 the supersaturation depletion due to vapor condensation. For monodisperse cloud droplets $q_l =$
 $(4/3)\pi\rho_w r_d^3 n_d$ where r_d is the radius of cloud droplet and n_d is number concentration in units
 110 of kg^{-1} . Thus, $dq_l/dt = 4\pi\rho_w n_d r_d^2 dr_d/dt = 4\pi\rho_w n_d r_d G s$. Here we use the linear growth for an
 individual droplet: $r_d dr_d/dt = G s$, where G is the condensation growth parameter (see Appendix).
 By setting the production and depletion terms on the right side of Equation 1 equal to each other, we
 obtain the quasi-stationary supersaturation within the cloud parcel:

$$s_{qs} = \frac{Aw}{r_d n_d}, \quad (2)$$

115 where A is a parameter depending on G , Q_1 and Q_2 (see Appendix).

The linear growth rate of cloud droplets in the quasi-stationary region is

$$r_d \frac{dr_d}{dt} = G s_{qs}. \quad (3)$$

Combining Equations 2, 3 and the definition of liquid water mixing ratio q_l for monodisperse
 120 droplets, we can get the linear growth rate of q_l ,

$$\frac{dq_l}{dt} = C_1 w, \quad (4)$$

where $C_1 = Q_1/Q_2$ with the units of m^{-1} (see Appendix). If we assume C_1 is a constant, then q_l
 can be derived by integration of Equation 4,

$$q_l = C_1 z + q_{l,i}, \quad (5)$$

125 where $q_{l,i}$ is the initial liquid water mixing ratio, and $z = \int w dt$ is the displacement of the cloud
 parcel away from its initial location. The liquid water mixing ratio increases linearly with height and



does not depend on the updraft velocity. It should be mentioned that Equation 5 describes q_l under thermodynamic equilibrium conditions. In reality, a cloud system needs some time (phase relaxation time) to reach the equilibrium state; For liquid clouds the phase relaxation time is usually smaller
130 than 10 s (Korolev and Mazin, 2003).

During the adiabatic process, two physical properties of the cloud parcel will be conserved: total water mass mixing ratio and liquid water potential temperature (Gerber et al., 2008), such that

$$q_{l,i} + q_{v,i} = q_{l,f} + q_{v,f} \quad (6)$$

135 and

$$T_i - \frac{l_w}{c_p \epsilon} q_{l,i} = T_f - \frac{l_w}{c_p \epsilon} q_{l,f} \quad (7)$$

where q is the water mass mixing ratio, T is temperature, l_w is the latent heat of liquid water and c_p is the specific heat of air at constant pressure. Subscripts l and v represent liquid and water vapor, respectively, while subscripts i and f denote the initial and final states of the cloud parcel. We note
140 that, for simplicity, the linearized form of the liquid water potential temperature has been used in Equation .

2.2 Liquid water mixing ratio in an adiabatic cloud after mixing

Now we consider the mixing of a cloud with dry and clean (aerosol free) environmental air and
145 subsequent evolution for a closed, rising parcel. We define the mixing fraction as χ , such that χ fraction of cloud air is mixed with $(1 - \chi)$ fraction of environmental air. We assume the mixing process is isobaric, and that the time scale for the mixing is much smaller than the time scale for the response of the cloud droplets during the mixing (i.e., homogeneous mixing limit). Therefore after isobaric mixing but before any phase changes, the liquid water mixing ratio should be $q_{l,im} = \chi q_{l,i}$
150 and the water vapor mixing ratio should be $q_{v,im} = \chi q_{v,i} + (1 - \chi) q_{v,e}$ and the temperature of the mixed parcel should be $T_{im} = \chi T_i + (1 - \chi) T_e$. The subscript im represents the initial state of mixed parcel (before the evaporation of cloud droplets in the mixed parcel) and subscript e denotes the state of the environmental air. After the mixing, we assume the mixed parcel rises adiabatically again with a constant updraft velocity w_m . For the purposes of this derivation w_m is prescribed and we
155 do not consider the actual buoyancy of the mixed parcel with respect to the environment. Similar to Equation 6 and 2.1, we have two conservation equations that allow the liquid water mixing ratio and temperature to be determined for the final state of the mixed parcel (Kumar et al., 2014), denoted by subscript fm :

$$\chi(q_{l,i} + q_{v,i}) + (1 - \chi)q_{v,e} = q_{l,fm} + q_{v,fm} \quad (8)$$



160 and

$$\chi T_i + (1 - \chi) T_e - \frac{l_w \chi}{c_p \epsilon} q_{l,i} = T_{fm} - \frac{l_w}{c_p \epsilon} q_{l,fm}. \quad (9)$$

Now we ask, how does the liquid water mixing ratio in the mixed parcel ($q_{l,fm}$) change with
 165 height above the mixing level? What is the difference of liquid water mixing ratio in the mixing
 parcel ($q_{l,fm}$) compared with that in the original parcel without mixing ($q_{l,f}$) at the same height?
 How does the difference ($q_{l,f} - q_{l,fm}$) change with height? To calculate this difference, we first
 subtract Equation 8 from Equation 6 to get the liquid water difference for the final state,

$$q_{l,f} - q_{l,fm} = (1 - \chi)(q_{l,i} + q_{v,i} - q_{v,e}) - (q_{v,f} - q_{v,fm}). \quad (10)$$

170 The first term on the right side is the total water mixing ratio difference between the original and new
 parcel, which depends on the initial condition of the parcel ($q_{l,i}, q_{v,i}$), the environmental air ($q_{v,e}$),
 and the mixing fraction χ . This difference is large when χ is small and environmental air is dry. The
 second term on the right side is the water vapor mixing ratio difference. The water vapor mixing
 ratio can be calculated from temperature, pressure and saturation ratio: $q_v = \frac{S e_s(T) \epsilon}{p - e_s(T)}$. Therefore the
 175 difference of water vapor mixing ratio is

$$q_{v,f} - q_{v,fm} = \frac{S_f e_s(T_f) \epsilon}{p_f - e_s(T_f)} - \frac{S_{fm} e_s(T_{fm}) \epsilon}{p_{fm} - e_s(T_{fm})}. \quad (11)$$

This equation is accurate but not simple enough to be useful. To achieve an analytical result, we
 first assume $p_f \approx p_{fm}$ because both parcels are at the same height. Secondly, we ignore e_s in the
 denominator because $p \gg e_s$. In addition, we assume both parcels are in quasi-steady state at that
 180 level and that the quasi-stationary supersaturation is much smaller than 1, so that the influence of the
 change of s_{qs} can be ignored compared with the change of $e_s(T)$ due to temperature; thus we assume
 $S_{fm} \approx S_f$. The main difference in the q_v arise from $e_s(T)$ due to the temperature differences. Using
 the linearized form of the Clausius-Clapeyron equation, we can approximate the difference of $e_s(T)$
 as

$$185 \quad e_s(T_f) - e_s(T_{fm}) \approx \frac{e_s(T_f) l_w}{p_f R T_f^2} (T_f - T_{fm}). \quad (12)$$

From the above assumptions and Equation 12, we can simplify Equation 11,

$$q_{v,f} - q_{v,fm} \approx \frac{S_f e_s(T_f) l_w \epsilon}{p_f R T_f^2} (T_f - T_{fm}). \quad (13)$$

Combining Equations 10 and 13, we find that the liquid water mixing ratio difference depends on
 the temperature difference in this way,

$$190 \quad q_{l,f} - q_{l,fm} = (1 - \chi)(q_{l,i} + q_{v,i} - q_{v,e}) - \frac{S_f e_s(T_f) l_w \epsilon}{R T_f^2} (T_f - T_{fm}). \quad (14)$$



In addition, the difference in liquid water potential temperature conservation equations for closed and mixed parcels given by Equation 2.1 minus Equation 9, leads to

$$(1 - \chi)(T_i - T_e - \frac{l_w}{c_p \epsilon} q_{l,i}) = T_f - T_{fm} - \frac{l_w}{c_p \epsilon} (q_{l,f} - q_{l,fm}). \quad (15)$$

Finally, from Equations 14 and 15, we can obtain the approximate solutions for liquid water mixing ratio difference and temperature difference,

$$q_{l,f} - q_{l,fm} = (1 - \chi) \frac{(1 + C_3)q_{l,i} + q_{v,i} - q_{v,e} - C_2(T_i - T_e)}{1 + C_3} \quad (16)$$

and

$$T_f - T_{fm} = (1 - \chi) \frac{C_2(T_i - T_e) + C_3(q_{v,i} - q_{v,e})}{C_2(1 + C_3)}. \quad (17)$$

Finally, combining Equations 5 and 16, we can get the liquid water profile for the mixed parcel,

$$q_{l,fm}(z) = C_1 z + q_{l,i} - (1 - \chi)K_1, \quad (18)$$

where $K_1 = ((1 + C_3)q_{l,i} + q_{v,i} - q_{v,e} - C_2(T_i - T_e))/(1 + C_3)$. It is interesting to see that the liquid water mixing ratio for the mixed parcel still increases linearly with height, but with a smaller value compared with an unmixed parcel (cf. Equation 5). The difference is the same at different heights, and is proportional to $1 - \chi$.

205

2.2.1 Total evaporation and reactivation height

Another way to look at Equation 18 is that the liquid water mixing ratio in the mixing parcel $q_{l,fm}$ increases with height linearly with the same slope as $q_{l,f}$ in the original parcel, but with a smaller initial liquid water mixing ratio in the mixing parcel $q_{l,im} = q_{l,i} - (1 - \chi)K_1$. Although the initial liquid water mixing ratio $q_{l,im}$ should be non-negative physically, $q_{l,i} - (1 - \chi)K_1$ can be negative mathematically. If $q_{l,im}$ is negative, it means that all cloud droplets evaporate. Therefore, $q_{l,i} = (1 - \chi)K_1$ is the criteria for critical condition that all droplets totally evaporate and the air in mixing parcel is just saturated. It is not difficult to prove that this critical condition is consistent with that given by Pinsky et al. (2015b), with $\gamma = 0$.

215

Even if $q_{l,im}$ is negative at $z = 0$, it can become positive at higher altitude. The negative value of $q_{l,im}$ at the beginning is the result of total evaporation, while the point where $q_{l,im}$ changes to positive can be taken to represent the re-activation of cloud condensation nuclei to form cloud droplets. The re-activation height z_{react} is the distance between the mixing level and the level at which $q_{l,im} = 0$, given by

$$z_{react} = \frac{(1 - \chi)K_1 - q_{l,i}}{C_1}. \quad (19)$$



2.2.2 Critical height for superadiabatic droplet growth

225 In this subsection we consider how cloud droplet size changes with height above the mixing level.
We consider an initially-adiabatic cloud parcel mixed isobarically with clean environmental air at
some level above the cloud base. Without vertical movement, the liquid water mixing ratio and
cloud number concentration will decrease due to dilution (not considering, for the moment, scenar-
ios in which all droplets are evaporated). The mean cloud droplet size after the response to mixing is
230 the same for extremely inhomogeneous mixing, but smaller for homogeneous mixing. If the parcel
still rises adiabatically after mixing, however, the liquid water mixing ratio will increase with height
(cf. Equation 18). This indicates that cloud droplet size will also increase with height, because the
number concentration does not change during the vertical motion. We now consider the growth of
cloud droplets under quasi-steady conditions. Because the cloud droplet concentration is smaller in
235 the mixed parcel than in the original parcel, s_{qs} in the mixed parcel will be larger ($s_{qs} \propto (r_{ad})^{-1}$,
see Equation 2). This implies that cloud droplets in the mixing parcel grow faster than those in
the original one due to higher supersaturation. This suggests that although cloud droplet size in the
mixed parcel is smaller for homogeneous mixing at the beginning, it might, with adequate vertical
displacement, become equal to or even larger than that in the original, unmixed parcel. The resulting
240 droplets would appear to have experienced super-adiabatic growth compared to a closed parcel. This
general picture of large-drop production resulting from decreased competition in diluted parcels has
been discussed elsewhere in the literature (Paluch and Knight, 1986; Cooper et al., 2013; Schmeiss-
ner et al., 2015).

245 We define the critical height z^* as the height when droplets in both parcels have the same sizes.
Based on the definition of liquid water mixing ratio, it is apparent that $q_{l,fm}/q_{l,f} = \chi$ at the critical
height, and therefore

$$\frac{C_1 z^* + q_{l,i} - (1 - \chi)K_1}{C_1 z^* + q_{l,i}} = \chi. \quad (20)$$

Solving Equation 20, we obtain

250
$$z^* = \frac{K_1 - q_{l,i}}{C_1}. \quad (21)$$

We note with interest that z^* is independent of the mixing fraction χ . Equations 18 and 21 indicate
that although the liquid water mixing ratio for the mixed parcel is always lower than that in the orig-
inal parcel, droplet radius in the mixed parcel will be larger than that in the original parcel when the
parcel is above z^* .

255



3 Results from parcel model

The analytical results derived in Section 2 have provided insight into the evolution of a cloud parcel after a mixing event, but several assumptions and simplifications were made, and some limitations such as perfectly clean (aerosol free) environment were imposed. We now explore the same concept of idealized mixing and subsequent-growth, but using an adiabatic parcel model with bin microphysics. The model was originally developed by Feingold et al. (1998) to simulate warm cloud process and has been applied to a wide range of microphysical problems (Feingold and Kreidenweis, 2000; Xue and Feingold, 2004; Ervens et al., 2005; Ervens and Feingold, 2012; Yang et al., 2012; Li et al., 2013). To study the mixing process, we add an idealized entrainment/detrainment and mixing process to the model. Entrainment means some fraction of environment air flows into the cloud, while detrainment means some fraction of cloud flows into the environment (de Rooy et al., 2013). The mixing process is implemented so that the entrained environmental air is homogeneously mixed with the remaining cloud body, and in all cases considered here this mixing level is set to 665 m (50 m above cloud base). It should be mentioned that mixing process might not necessarily happen when entrainment/detrainment occurs. The time interval between these two processes is called the mixing time scale, and the presence of a delay would be expected for inhomogeneous mixing. The relative magnitudes of this mixing time scale and the phase relaxation time determine whether the mixing occurs in the homogeneous or inhomogeneous limit (e.g., Baker et al., 1980). To be consistent with the previous theoretical development (Sec. 2) we implement the homogeneous mixing limit within the model, i.e., the instantaneous exposure of droplets to the mixture of cloudy and entrained air. This implies that the turbulent mixing time is very small compared to the phase relaxation time, and is therefore similar to the limit considered by Pinsky et al. (2015b).

Initial conditions for the parcel are $z_0 = 300$ m, $p_0 = 919$ Pa, $T_0 = 288.15$ K and $RH_0 = 85\%$. Cloud condensation nuclei (CCN) are ammonium sulfate particles with a monodisperse radius of 50 nm and concentration of 50 mg^{-1} . The parcel rises adiabatically with constant updraft velocity. Two updraft velocities (w) are chosen in this study: 0.1 and 1.0 m s^{-1} . Observation results show that updraft velocity in cumulus cloud is on the order of 1.0 m s^{-1} , and that for stratocumulus cloud is on the order of 0.1 m s^{-1} (Katzwinkel et al., 2014; Ditas et al., 2012). Cloud base is reached at $z = 615$ m, where CCN are activated as cloud droplets. The isobaric mixing process occurs at $z = 665$ m, 50 m above the cloud base. For simplicity, we assume the environmental temperature at the mixing level is the same as that of the cloud parcel, but the relative humidity is only 85%. After the mixing, the new mixed parcel rises adiabatically again with the same updraft velocity.

Liquid water mixing ratio profiles for six different mixing fractions $\chi = 1.0, 0.9, 0.8, 0.7, 0.6, 0.5$ at $w = 0.1 \text{ m s}^{-1}$ are shown in Figure 1 (a). The analytical results based on Equation 18 are also shown and are quite close to the results from the parcel model. As seen from Figure 1 (a), the liquid



water mixing ratio for smaller χ is smaller than that for larger χ at the same height. In addition, when $\chi \leq 0.8$, the liquid water mixing ratio will decrease to zero at the beginning, which means that the
295 cloud totally evaporates and becomes subsaturated. It should be mentioned that in the model each cloud droplet contains one CCN, and when a cloud droplet totally evaporates the CCN still survives. Because the subsaturated parcel still rises adiabatically, CCN in the mixing parcel can be activated again when the air becomes saturated at a higher level, which we defined as the re-activation level. The smaller χ is, the higher the re-activation level is. The evaporation and re-activation processes can
300 be clearly seen from the cloud droplet radius profile in Figure 1 (b). In addition, it clearly shows that the mixed cloud parcel can reach super-adiabatic growth conditions (where the cloud droplet radius in the mixed parcel is larger than that in the original, unmixed parcel with $\chi = 1.0$) above a critical height. The critical height is independent of χ and agrees well with that predicted by Equation 21.

305 Results above are for a cloud parcel mixing with clean environmental air (aerosol free condition). However, both observational and modeling results show that air around the cumulus cloud is usually not clean (Katzwinkel et al., 2014; Chen et al., 2012). There can be background aerosols in the atmosphere even at high altitude, and in addition, subsiding shells can also provide sufficient aerosols as CCN when mixing occurs (Heus and Jonker, 2008). There is no simple analytical result for mixing
310 with a polluted environment. However, we can use the parcel model to investigate the effect of mixing when the environmental air is polluted. For simplicity, we assume the environment has the same dry aerosol size distribution as that below the cloud base.

Figure 1 (c) shows the monodisperse cloud droplet radius versus height for various χ after mixing
315 with a polluted environment at $w = 0.1 \text{ m s}^{-1}$. For $\chi = 0.9$, the remaining cloud droplets do not totally evaporate and the entrained aerosols are not activated as cloud droplets. For smaller χ , the remaining cloud droplets totally evaporate and leave CCN in the mixed parcel. Both entrained and remaining CCN are activated at a higher level. In addition, only the parcel with $\chi = 0.9$ can reach the super-adiabatic growth region. For smaller χ , cloud droplets are smaller than those in the original
320 parcel at the same height z^* . This is similar to the aerosol indirect effect in which more aerosols leads to smaller cloud droplets. In summary, when mixing with a polluted environment, the mixing parcel can reach super-adiabatic growth conditions at the predicted z^* only if the cloud does not totally evaporate after mixing.

325 Figure 2 (a) and (b) show the results for mixing with a clean environment at larger updraft velocity $w = 1.0 \text{ m s}^{-1}$. It can be seen that the liquid water mixing ratio and cloud droplet radius profiles are almost the same compared with Figure 1, except that the mixing parcel totally evaporate for $\chi = 0.8$ at $w = 0.1 \text{ m s}^{-1}$, but doesn't totally evaporate for $\chi = 0.8$ at $w = 1.0 \text{ m s}^{-1}$. This is because larger updraft velocity supplies more water within the fixed phase relaxation time, so droplets begin to grow



330 before they have had time to completely evaporate. The mixed parcel can reach the super-adiabatic growth region when it is above z^* . And as before, z^* is independent of both mixing fraction and updraft velocity, consistent with the theoretical prediction.

When mixing with polluted environment air at $w = 1.0 \text{ m s}^{-1}$, the mixed parcel can't reach the
335 super-adiabatic growth region whether the mixing parcel totally evaporates or not (see Figure 2 (c)). The reason is that with large updraft velocity, the entrained CCN can always be activated as cloud droplets, thus compete for water vapor in the mixed parcel. It should be mentioned that results here strongly depend on the physical and chemical properties of the entrained CCN, e.g. sizes, chemical composition, and number concentration. For example, the mixed parcel might also reach the super-
340 adiabatic growth region if the environmental air only contains a small number of CCN. In general, however, mixing with polluted air will inhibit the super-adiabatic growth of cloud droplets.

Cloud droplets in a real cloud are usually polydisperse and we now consider to what extent the theoretical predictions apply in this more complex system. The effect of mixing on a polydisperse
345 droplet population is tested with the cloud parcel model. The initial aerosols are composed of ammonium sulfate and are distributed lognormally in 20 bins with 50 nm median radius, standard deviation of 1.4, and a total number concentration of 100 cm^{-3} . Initial radii of the dry aerosols for the 20 bins are listed in Table 2. The cloud droplet diameters for each bin versus height for $\chi = 0.9, 0.7, 0.5$ are shown in Figure 3. These results are for clean environmental air and $w = 0.1 \text{ m s}^{-1}$ and are representative of the other cases. It can be seen that not all 20 bins are activated at cloud base; for example,
350 only the largest 11 aerosol sizes are activated as cloud droplets for $\chi = 1.0$. Cloud droplets evaporate a little bit for $\chi = 0.9$, or completely for $\chi = 0.7, 0.5$, and re-activation occurs again at a higher level. It is very interesting to see that for $\chi = 0.5$, the 12th bin is not activated at cloud base, but is activated for the first time after mixing (green line). This asymmetric phenomenon is due to the significant
355 reduction of cloud droplet number concentration after mixing. Thermodynamic equilibrium predicts how much water vapor should condense at a certain level, but mixing with a clean environment reduces the overall CCN concentration. To condense the same amount of water, either the single droplets must grow larger than before, which is the physical explanation for super-adiabatic growth; or some initially un-activated aerosol particles can be activated to increase the cloud number
360 concentration.

Super-adiabatic droplet growth for individual droplet size bins can be observed in Figure 3, but it is achieved at different heights above the mixing level. Figure 4 shows these critical heights for individual cloud droplet size bins calculated from the cloud parcel model for the various mixing
365 fractions. Here again, the environmental air is clean with $T_e = T_c$ and $RH_e = 85\%$. We note that cloud droplet size decreases with increasing bin number (i.e., cloud droplet size increases with in-



creasing dry aerosol size, as expected). The critical height for each bin is defined when the sizes of cloud droplets for that bin are equal for both mixed and unmixed cloud parcels. It can be seen that the critical height depends on the size of the cloud droplet, the mixing fraction and the updraft velocity, especially for low updraft velocity $w = 0.1 \text{ m s}^{-1}$. For $w = 1.0 \text{ m s}^{-1}$, critical heights for individual bins are close to the theoretical critical height for a monodisperse cloud droplet population. In the low updraft speed case (left panel) it is particularly striking that the $\chi = 0.9$ curve has a different dependence than that for the other mixing fractions: increasing rather than decreasing z^* with decreasing droplet size. We believe the explanation is that the $\chi = 0.9$ case is the only scenario in which complete droplet evaporation does not occur. Thus, the presence of complete evaporation and subsequent re-activation changes the population dynamics of the cloud substantially for low updraft speeds. Although the critical heights are different for individual size bins, we might expect that the simple monodisperse prediction for z^* would hold for some moment of cloud droplet size distribution. Considering that the thermodynamically-predicted water mass is distributed over a variable number of aerosol particles, the most logical choice is a prediction of z^* using the volume-mean radius. Figure 5 shows the volume-weighted mean radius as a function of height for six values of χ and for updraft speeds of 0.1 and 1.0 m s^{-1} . In spite of the complex behavior observed for individual bins, the volume-mean radius curves are observed to cross at nearly the same height and with very close agreement with the analytical prediction. This suggests that the theory can be applied under realistic cloud conditions with polydisperse droplet populations.

4 Discussions and conclusions

In this study, we have considered isobaric mixing of a cloud parcel with environmental air, and then the subsequent droplet growth as the parcel rises adiabatically afterwards. Analytical expressions are derived for monodisperse cloud droplets when mixing with clean environmental air. Results show that the liquid water mixing ratio q_l in the mixed parcel increases linearly with height with the same slope ($\frac{dq_l}{dz}$) as the original parcel (without mixing). Due to the mixing the q_l is smaller compared with the unmixed parcel at the same height. A closed form expression for the offset is derived and shows that the decrease of q_l in the mixed parcel depends on the mixing fraction χ and the temperature and relative humidity of the environmental air. A critical height z^* , defined as the height at which the cloud droplet sizes are equal in both mixed and original cloud parcels, is derived. Interestingly, the critical height depends on the initial conditions of the cloud and environmental air, but is independent of the mixing fraction. Cloud droplets in the mixed parcel are larger than in the original parcel above z^* , which we call the “super-adiabatic” growth region. These large cloud droplets may help explain the formation of initial large droplets that contribute to precipitation formation in warm



clouds.

The predicted vertical profile of liquid water mixing ratio and the critical height are confirmed using a bin microphysical cloud model. For large χ and a humid environment, cloud droplets will evaporate a little bit and grow again after mixing. For small χ and dry environment, cloud droplets can evaporate completely, leaving the mixed parcel subsaturated. Droplets are re-activated at a higher level, as long as the mixing parcel rises sufficiently to reach saturation again. The theoretical predictions are based on equilibrium arguments, but because the phase relaxation time is typically short for warm clouds, results are not very sensitive to updraft speed over the range investigated. For monodisperse cloud droplets, z^* is independent of mixing fraction and updraft speed. For polydisperse cloud droplets, however, z^* defined for individual droplet sizes is observed to depend on droplet size, mixing fraction and updraft velocity, especially for smaller w . For larger w , z^* is insensitive to those variables and close to the analytical result for monodisperse cloud droplets. The situation becomes much simpler and the polydisperse cloud can be predicted theoretically by using the volume-mean cloud droplet radius. Finally, we note that the model results presented here are for the condition of cloud and environment having the same temperature; model runs for other reasonable conditions also produced good agreement with the theory.

Environment background aerosols and subsiding shells may contain effective CCN that can be activated after mixing, thus inhibiting super-adiabatic droplet growth. For large updraft speed, the entrained aerosols can be activated as cloud droplets, thus increasing cloud droplet concentration and decreasing the cloud droplet sizes. For small updraft velocity, the mixed parcel can reach the super-adiabatic growth region only when the entrained aerosols cannot be activated and the cloud droplets do not totally evaporate. Otherwise if cloud droplets totally evaporate, both remaining and entrained CCN can be activated when the mixed parcel is saturated again. If the entrained aerosols can be activated as cloud droplets, the mixed parcel usually contains smaller cloud droplets, but similar number concentration compared with the main cloud body. This might help explain the observation that some cloud samples appear to be undiluted in droplet number concentration, but have significantly smaller mean-volume radii, a region otherwise outside the homogeneous mixing limiting curve in a mixing diagram (Schmeissner et al., 2015).

Given the success of the analytical results in predicting the critical height z^* above which volume-weighted mean droplet diameters will appear to be super-adiabatic, we briefly explore the dependence of z^* on environmental conditions. As noted already, and now confirmed by the parcel model, the critical height does not depend on mixing fraction χ or on the updraft speed w . As seen in Figure 6, z^* changes with the relative humidity of the environmental air (RH_e) at the mixing level. It can be seen that z^* decreases as RH_e increases. For example, when $RH_e = 98\%$, z^* is less than 50



m above the mixing level. This means that the mixed parcel can reach the super-adiabatic growth region more easily when mixing with a humid environment. In the real atmosphere, the subsiding
440 shell around a cumulus cloud in a clean environment might be very humid due to the evaporation of cloud droplets at higher cloud levels. Mixing under these conditions would be favorable for super-adiabatic growth of cloud droplets, especially if the subsiding shell has been cleared for most CCN through scavenging.

445 The results presented here all are for the homogeneous mixing limit. It is possible to develop model prescriptions for extreme inhomogeneous mixing, but our sense is that the results would be sensitive to the necessarily artificial nature of those prescriptions. Ultimately, a realistic model or a direct numerical simulation of the mixing process are required for the inhomogeneous limit. We can speculate, however, that the results obtained here would only be amplified for inhomogeneous
450 mixing: in that limit the droplet concentration is reduced but the mean volume diameter remains unchanged, implying that z^* is zero and super-adiabatic droplet growth can begin immediately after the mixing process has concluded. By concluded we mean that the cloudy and environmental air have become completely mixed, leaving a spatially homogeneous field of droplets having the same diameter as before mixing, but lower number concentration due to dilution and total evaporation of
455 some subset of droplets (e.g., Beals et al., 2015). This neglects the more complicated interactions that might come into play if CCN are entrained during mixing with environmental air: in that case activation of new CCN may occur as the parcel rises, even before complete mixing to the microscale has taken place.

A crucial factor that has not been considered thus far is the influence of mixing on the vertical
460 motion of a cloud parcel due to changes in its buoyancy. Whether a mixed cloud parcel can experience super-adiabatic droplet growth depends not only on the critical height z^* , but also on the maximum height z_{max} it can reach after mixing: a cloud can reach the super-adiabatic growth region only for $z_{max} > z^*$. Calculation of z_{max} is nontrivial because one must consider the time dependence of the buoyancy, drag force, and kinetic energy of the parcel, which depends on the properties of the
465 surrounding environment and its dependence on height. These are still open research problems (e.g., slippery versus sticky thermals (Sherwood et al., 2013; Romps and Charn, 2015)), so exploring this important aspect is beyond the scope of our paper; but qualitatively, our results imply that strongly convective clouds may favor super-adiabatic growth compared to weakly convective clouds. In addition, decreasing χ will tend to decrease the buoyancy and therefore the updraft speed, thus
470 ultimately decreasing z_{max} . Therefore, it is more likely to reach the super-adiabatic droplet growth region for larger χ , again favoring clouds in humid environments or clouds with well developed, humid subsiding shells.



In a real cloud the liquid water mixing ratio profile is much more complicated than considered
475 here. Mixing will occur at different levels and environmental conditions change with height. There
are several methods to predict the mixing fraction at different levels. For example, Lu et al. (2012)
predict χ using the cloud base condition, liquid water mixing ratio and environmental condition at
each level. The advantage of their method is that they do not need to measure temperature and water
vapor mixing ratio in the cloud, which have significant measurement uncertainty. Here, we have pro-
480 vided an explicit method to estimate the mixing fraction at each level using a similar strategy. Based
on Equation 16 and 17, we can also calculate the mixing fraction profile. The key difference is that
our method is explicit, while their method is implicit.

The central insights of this work are that a mixed parcel is more likely to reach the super-adiabatic
485 growth region when convection is strong, and the environmental air is humid and clean. Cloud
droplets in the super-adiabatic growth region are larger than that in an unmixed parcel. Our hope
is that the theoretical results obtained here and confirmed with the parcel model, can help in evaluat-
ing the possible role of mixing-induced droplet growth for large droplet production and development
of precipitation in warm clouds.

490 *Acknowledgements.* This research was supported by the DOE Office of Science as part of the Atmospheric
System Research program through Grant No. DE-SC0011690.



Appendix A: List of Symbols

Table 1. List of Symbols

Symbol	Description	Units
A	$\frac{Q_1}{4\pi\rho_w G Q_2}$	s kg^{-1}
c_p	specific heat of air at constant temperature	J mol^{-1}
C_1	$4\pi\rho_w G A = Q_1/Q_2$	m^{-1}
C_2	$\frac{S_f e_s (T_f) l_w \epsilon}{p_f R T_f^2}$	K^{-1}
C_3	$\frac{C_2 l_w}{c_p \epsilon}$	–
D_v	Diffusivity of water vapor	$\text{m}^2 \text{s}^{-1}$
e_v	water vapor pressure	Pa
$e_s(T)$	saturated water vapor pressure at temperature T	Pa
G	$\left[\frac{\rho_w R T}{M_w D_v e_s(T)} + \frac{\rho_w l_w}{M_w k T T} \left(\frac{l_w}{R T} - 1 \right) S \right]^{-1}$	$\text{m}^2 \text{s}^{-1}$
k_T	coefficient of air heat conductivity	$\text{J m}^{-1} \text{s}^{-1}$
K_1	$\frac{(1+C_3)q_{l,i}+q_{v,i}-q_{v,e}-C_2(T_i-T_e)}{1+C_3}$	–
K_2	$\frac{C_2(T_i-T_e)+C_3(q_{v,i}-q_{v,e})}{C_2(1+C_3)}$	K
l_w	latent heat of liquid water	J mol^{-1}
M_{air}	molar mass of air	kg mol^{-1}
M_w	molar mass of water	kg mol^{-1}
n_d	droplet number per unit mass of air	kg^{-1}
q_l	liquid water mixing ratio	–
$q_{l,i}$	initial q_l	–
$q_{l,im}$	initial q_l with mixing fraction χ	–
$q_{l,f}$	final q_l	–
$q_{l,fm}$	final q_l with mixing fraction χ	–
q_v	water vapor mixing ratio	–
$q_{v,e}$	environmental q_v	–
$q_{v,i}$	initial q_v	–
$q_{v,im}$	initial q_v with mixing fraction χ	–
$q_{v,f}$	final q_v	–
$q_{v,fm}$	final q_v with mixing fraction χ	–
Q_1	$(l_w/(c_p T) - 1)(M_{air}g/RT)$	m^{-1}
Q_2	$\rho_{air} l_w^2 / (M_w p c_p T) + \rho_{air} R T / (M_w e_s(T))$	–
r_d	radius of cloud droplet	m
$r_{d,i}$	initial r_d	m
$r_{d,f}$	final r_d	m
$r_{d,fm}$	final r_d with mixing fraction χ	m
R	universal gas constant	$\text{J mol}^{-1} \text{K}^{-1}$
s	$S - 1$, water vapor supersaturation	–
S	$\frac{e_v}{e_s}$, water vapor saturation ratio	–
S_f	final S	–
S_{fm}	final S with mixing fraction χ	–
T	temperature	K
T_i	initial T	K
T_{im}	initial T with mixing fraction χ	K
T_e	environmental T	K
T_f	final T	K
T_{fm}	final T with mixing fraction χ	K
w	updraft velocity of cloud parcel	m s^{-1}
w_m	updraft velocity of cloud parcel with mixing fraction χ	m s^{-1}
χ	isobaric mixing fraction	–
ϵ	$\frac{M_w}{M_{air}}$	–
κ	$\frac{R}{c_p}$	–
ρ_w	density of liquid water	kg m^{-3}
ρ_{air}	density of air	kg m^{-3}



References

- Andrejczuk, M., Grabowski, W. W., Malinowski, S. P., and Smolarkiewicz, P. K.: Numerical simulation of
495 cloud-clear air interfacial mixing: Effects on cloud microphysics, *Journal of the atmospheric sciences*, 63,
3204–3225, 2006.
- Andrejczuk, M., Grabowski, W. W., Malinowski, S. P., and Smolarkiewicz, P. K.: Numerical simulation of
cloud-clear air interfacial mixing: homogeneous versus inhomogeneous mixing, *Journal of the Atmospheric
Sciences*, 66, 2493–2500, 2009.
- 500 Baker, M., Corbin, R., and Latham, J.: The influence of entrainment on the evolution of cloud droplet spectra: I.
A model of inhomogeneous mixing, *Quarterly Journal of the Royal Meteorological Society*, 106, 581–598,
1980.
- Beals, M. J., Fugal, J. P., Shaw, R. A., Lu, J., Spuler, S. M., and Stith, J. L.: Holographic measurements of
inhomogeneous cloud mixing at the centimeter scale, *Science*, 350, 87–90, 2015.
- 505 Beard, K. V. and Ochs III, H. T.: Warm-rain initiation: An overview of microphysical mechanisms, *Journal of
Applied Meteorology*, 32, 608–625, 1993.
- Blyth, A. M., Lasher-Trapp, S. G., Cooper, W. A., Knight, C. A., and Latham, J.: The role of giant and ultragiant
nuclei in the formation of early radar echoes in warm cumulus clouds, *Journal of the atmospheric sciences*,
60, 2557–2572, 2003.
- 510 Burnet, F. and Brenguier, J.-L.: Observational study of the entrainment-mixing process in warm convective
clouds, *Journal of the atmospheric sciences*, 64, 1995–2011, 2007.
- Chen, G., Xue, H., Feingold, G., and Zhou, X.: Vertical transport of pollutants by shallow cumuli from large
eddy simulations, *Atmospheric Chemistry and Physics*, 12, 11 319–11 327, 2012.
- Chen, J., Liu, Y., and Zhang, M.: Investigation the influences of entrainment mixing processes on cloud micro-
physics using new cloud parcel model, AGU Fall Meeting, 2015.
- 515 Cheng, W. Y., Carrió, G. G., Cotton, W. R., and Saleeby, S. M.: Influence of cloud condensation and giant
cloud condensation nuclei on the development of precipitating trade wind cumuli in a large eddy simulation,
Journal of Geophysical Research: Atmospheres (1984–2012), 114, 2009.
- Cooper, W. A., Lasher-Trapp, S. G., and Blyth, A. M.: The influence of entrainment and mixing on the initial
520 formation of rain in a warm cumulus cloud, *Journal of the Atmospheric Sciences*, 70, 1727–1743, 2013.
- Cotton, W. R., Bryan, G., and Van den Heever, S. C.: *Storm and cloud dynamics*, vol. 99, Academic press, 2011.
- de Rooy, W. C., Bechtold, P., Fröhlich, K., Hohenegger, C., Jonker, H., Mironov, D., Pier Siebesma, A., Teixeira,
J., and Yano, J.-I.: Entrainment and detrainment in cumulus convection: an overview, *Quarterly Journal of
the Royal Meteorological Society*, 139, 1–19, 2013.
- 525 Ditas, F., Shaw, R. A., Siebert, H., Simmel, M., Wehner, B., and Wiedensohler, A.: Aerosols-cloud
microphysics-thermodynamics-turbulence: evaluating supersaturation in a marine stratocumulus cloud, *At-
mospheric Chemistry and Physics*, 12, 2459–2468, 2012.
- Ervens, B. and Feingold, G.: On the representation of immersion and condensation freezing in cloud models
using different nucleation schemes, *Atmospheric Chemistry and Physics*, 12, 5807–5826, 2012.
- 530 Ervens, B., Feingold, G., and Kreidenweis, S. M.: Influence of water-soluble organic carbon on cloud drop
number concentration, *Journal of Geophysical Research: Atmospheres (1984–2012)*, 110, 2005.



- Feingold, G. and Kreidenweis, S.: Does cloud processing of aerosol enhance droplet concentrations?, *Journal of Geophysical Research: Atmospheres* (1984–2012), 105, 24 351–24 361, 2000.
- Feingold, G., Walko, R., Stevens, B., and Cotton, W.: Simulations of marine stratocumulus using a new micro-
535 physical parameterization scheme, *Atmospheric research*, 47, 505–528, 1998.
- Feingold, G., Cotton, W. R., Kreidenweis, S. M., and Davis, J. T.: The impact of giant cloud condensation nuclei
on drizzle formation in stratocumulus: Implications for cloud radiative properties, *Journal of the atmospheric
sciences*, 56, 4100–4117, 1999.
- Gerber, H., Frick, G., Jensen, J., and Hudson, J.: Entrainment, mixing, and microphysics in trade-wind cumulus,
540 *J. Meteor. Soc. Japan*, 86, 87–106, 2008.
- Göke, S., Ochs III, H. T., and Rauber, R. M.: Radar analysis of precipitation initiation in maritime versus
continental clouds near the Florida coast: Inferences concerning the role of CCN and giant nuclei, *Journal of
the Atmospheric Sciences*, 64, 3695–3707, 2007.
- Heus, T. and Jonker, H. J.: Subsiding shells around shallow cumulus clouds, *Journal of the Atmospheric Sci-
ences*, 65, 1003–1018, 2008.
545
- Hocking, L.: The collision efficiency of small drops, *Quarterly Journal of the Royal Meteorological Society*,
85, 44–50, 1959.
- Jensen, J., Austin, P., Baker, M., and Blyth, A.: Turbulent mixing, spectral evolution and dynamics in a warm
cumulus cloud, *Journal of the atmospheric sciences*, 42, 173–192, 1985.
- 550 Jensen, J. B. and Lee, S.: Giant sea-salt aerosols and warm rain formation in marine stratocumulus, *Journal of
the atmospheric sciences*, 65, 3678–3694, 2008.
- Johnson, D. B.: The role of giant and ultragiant aerosol particles in warm rain initiation, *Journal of the Atmo-
spheric Sciences*, 39, 448–460, 1982.
- Katzwinkel, J., Siebert, H., Heus, T., and Shaw, R. A.: Measurements of turbulent mixing and subsiding shells
555 in trade wind cumuli, *Journal of the Atmospheric Sciences*, 71, 2810–2822, 2014.
- Korolev, A., Pinsky, M., and Khain, A.: A New Mechanism of Droplet Size Distribution Broadening during
Diffusional Growth, *Journal of the Atmospheric Sciences*, 70, 2051–2071, 2013.
- Korolev, A., Khain, A., Pinsky, M., and J, F.: Theoretical analysis of mixing in liquid clouds–Part 1: Classical
concept, *Atmospheric Chemistry and Physics Discussions*, 15, 30 211–30 267, 2015.
- 560 Korolev, A. V. and Mazin, I. P.: Supersaturation of water vapor in clouds, *Journal of the atmospheric sciences*,
60, 2957–2974, 2003.
- Kostinski, A. B. and Shaw, R. A.: Fluctuations and luck in droplet growth by coalescence, *Bulletin of the
American Meteorological Society*, 86, 235–244, 2005.
- Kumar, B., Schumacher, J., and Shaw, R. A.: Lagrangian mixing dynamics at the cloudy-clear air interface,
565 *Journal of the Atmospheric Sciences*, 2014.
- Laird, N. F., Ochs Iii, H. T., Rauber, R. M., and Miller, L. J.: Initial precipitation formation in warm Florida
cumulus, *Journal of the atmospheric sciences*, 57, 3740–3751, 2000.
- Lamb, D. and Verlinde, J.: *Physics and chemistry of clouds*, Cambridge University Press, 2011.
- Lasher-Trapp, S. G., Cooper, W. A., and Blyth, A. M.: Broadening of droplet size distributions from entrainment
570 and mixing in a cumulus cloud, *Quarterly Journal of the Royal Meteorological Society*, 131, 195–220, 2005.



- Lehmann, K., Siebert, H., and Shaw, R. A.: Homogeneous and inhomogeneous mixing in cumulus clouds: dependence on local turbulence structure, *Journal of the Atmospheric Sciences*, 66, 3641–3659, 2009.
- Li, Z., Xue, H., and Yang, F.: A modeling study of ice formation affected by aerosols, *Journal of Geophysical Research: Atmospheres*, 118, 11–213, 2013.
- 575 Lozar, A. d. and Muessle, L.: Long-resident droplets at the stratocumulus top, *Atmospheric Chemistry and Physics Discussions*, 2016.
- Lu, C., Liu, Y., Yum, S. S., Niu, S., and Endo, S.: A new approach for estimating entrainment rate in cumulus clouds, *Geophysical Research Letters*, 39, 2012.
- Lu, C., Niu, S., Liu, Y., and Vogelmann, A. M.: Empirical relationship between entrainment rate and micro-
- 580 physics in cumulus clouds, *Geophysical Research Letters*, 40, 2333–2338, 2013.
- Magaritz-Ronen, L., Pinsky, M., and Khain, A.: Drizzle formation in stratocumulus clouds: effects of turbulent mixing, *Atmospheric Chemistry and Physics Discussions*, 15, 24 131–24 177, 2015.
- Naumann, A. K. and Seifert, A.: A Lagrangian drop model to study warm rain microphysical processes in a shallow cumulus, *Journal of Advances in Modeling Earth Systems*, 7, 1136–1154, 2015.
- 585 Paluch, I. R. and Knight, C. A.: Does mixing promote cloud droplet growth?, *Journal of the atmospheric sciences*, 43, 1994–1998, 1986.
- Pinsky, M., Khain, A., and Korolev, A.: Theoretical analysis of mixing in liquid clouds–Part 3: Inhomogeneous mixing, *Atmospheric Chemistry and Physics Discussions*, 15, 30 321–30 381, 2015a.
- Pinsky, M., Khain, A., Korolev, A., and L, M.-R.: Theoretical analysis of mixing in liquid clouds–Part 2: Ho-
- 590 mogeneous mixing, *Atmospheric Chemistry and Physics Discussions*, 15, 30 269–30 320, 2015b.
- Pruppacher, H. R., Klett, J. D., and Wang, P. K.: *Microphysics of clouds and precipitation*, Taylor & Francis, 1998.
- Romps, D. M. and Charn, A. B.: Sticky thermals: Evidence for a dominant balance between buoyancy and drag in cloud updrafts, *Journal of the Atmospheric Sciences*, 72, 2890–2901, 2015.
- 595 Schmeissner, T., Shaw, R., Ditas, J., Stratmann, F., Wendisch, M., and Siebert, H.: Turbulent Mixing in Shallow Trade Wind Cumuli: Dependence on Cloud Life Cycle, *Journal of the Atmospheric Sciences*, 72, 1447–1465, 2015.
- Sherwood, S. C., Hernández-Deckers, D., Colin, M., and Robinson, F.: Slippery Thermals and the Cumulus Entrainment Paradox*, *Journal of the Atmospheric Sciences*, 70, 2426–2442, 2013.
- 600 Tölle, M. H. and Krueger, S. K.: Effects of entrainment and mixing on droplet size distributions in warm cumulus clouds, *Journal of Advances in Modeling Earth Systems*, 6, 281–299, 2014.
- Wang, L.-P. and Grabowski, W. W.: The role of air turbulence in warm rain initiation, *Atmospheric Science Letters*, 10, 1–8, 2009.
- Xue, H. and Feingold, G.: A modeling study of the effect of nitric acid on cloud properties, *Journal of Geophysical Research: Atmospheres (1984–2012)*, 109, 2004.
- 605 Yang, F., Xue, H., Deng, Z., Zhao, C., and Zhang, Q.: A closure study of cloud condensation nuclei in the North China Plain using droplet kinetic condensational growth model, *Atmospheric Chemistry and Physics*, 12, 5399–5411, 2012.



610 Yin, Y., Levin, Z., Reisin, T. G., and Tzivion, S.: The effects of giant cloud condensation nuclei on the development of precipitation in convective clouds—A numerical study, *Atmospheric Research*, 53, 91–116, 2000.

Yum, S. S., Wang, J., Liu, Y., Senum, G., Springston, S., McGraw, R., and Yeom, J. M.: Cloud microphysical relationships and their implication on entrainment and mixing mechanism for the stratocumulus clouds measured during the VOCALS project, *Journal of Geophysical Research: Atmospheres*, 2015.

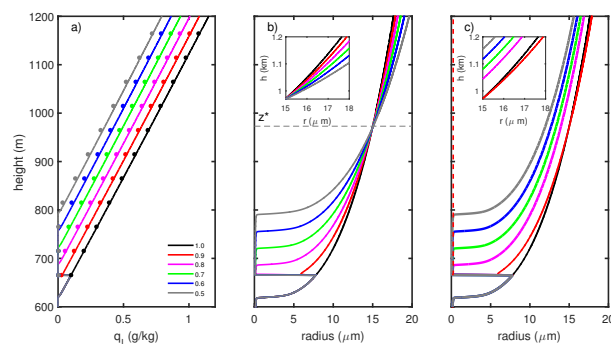


Figure 1. (a) Liquid water mixing ratio profiles for various cloud mixing fractions χ and with low updraft speed (0.1 m s^{-1}). Lines are from the parcel model and dots are from the theoretical prediction given by Equation 18. (b) Cloud droplet radius versus height for various χ when mixing with clean (aerosol free) environmental air. The horizontal dashed line represents the critical height z^* calculated from Equation 21. (c) Cloud droplet radius versus height for various χ when mixing with polluted environmental air (air containing CCN similar to cloud base conditions). Insets in (b) and (c) show details of the radius profiles above the critical height. Superadiabatic droplet growth, i.e. droplet diameters greater than in the unmixed cloud ($\chi = 1.0$), is observed for all χ in (b) and only for $\chi = 0.9$ in (c).

Table 2. Initial dry aerosols radii for different bins

Bin number	r_{dry} (nm)	Bin number	r_{dry} (nm)
1	463.7	11	61.5
2	378.9	12	50.3
3	309.6	13	41.1
4	253.0	14	33.6
5	206.7	15	27.4
6	168.9	16	22.4
7	138.0	17	18.3
8	112.8	18	15.0
9	92.1	19	12.2
10	75.3	20	10.0

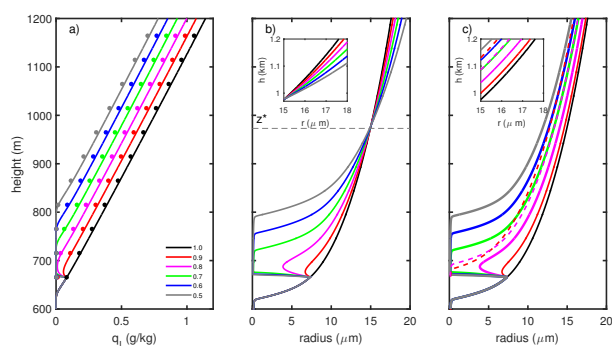


Figure 2. (a) Liquid water mixing ratio profiles for various cloud mixing fractions χ and with high updraft speed (1.0 m s^{-1}). Lines are from the parcel model and dots are from the theoretical prediction given by Equation 18. (b) Cloud droplet radius versus height for various χ when mixing with clean (aerosol free) environmental air. The horizontal dashed line represents the critical height z^* calculated from Equation 21. (c) Cloud droplet radius versus height for various χ when mixing with polluted environmental air (air containing CCN similar to cloud base conditions). Insets in (b) and (c) show details of the radius profiles above the critical height. Super-adiabatic droplet growth, i.e. droplet diameters greater than in the unmixed cloud ($\chi = 1.0$), is observed for all χ in (b) but for none in (c).

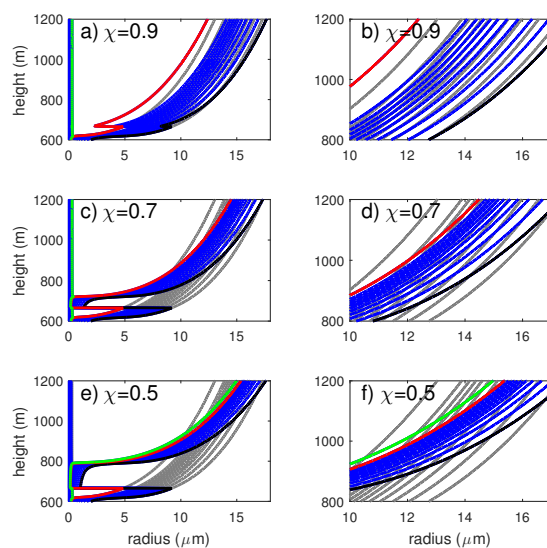


Figure 3. Radii of cloud droplets in a polydisperse population versus height for $\chi = 0.9, 0.7, 0.5$ in a clean environment at $w = 0.1 \text{ m s}^{-1}$. The background grey lines represent $\chi = 1.0$. The right column shows the region near the critical height where super-adiabatic growth can be expected. The black line is for the 1st bin (largest CCN), the red line for the 11th bin, and the green line for the 12th bin.

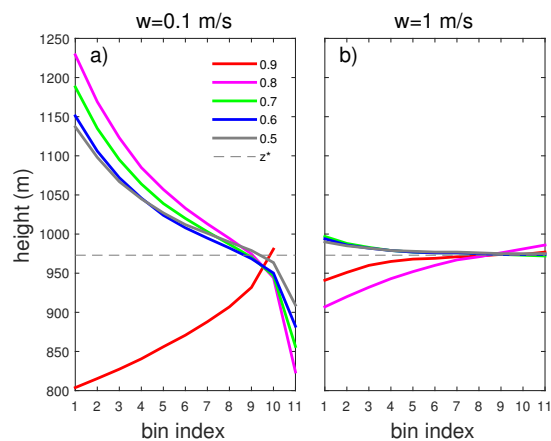


Figure 4. Critical height for individual droplet size bins for a polydisperse cloud droplet population calculated from cloud parcel model. Results are shown for two updraft velocities, (a) $w = 0.1 \text{ m s}^{-1}$ and (b) $w = 1.0 \text{ m s}^{-1}$. The line colors represent different mixing fractions χ as defined in the legend, and the dashed line is the analytical result for critical height z^* for a monodisperse cloud droplet population. Cloud droplet size decreases as the bin number increases.

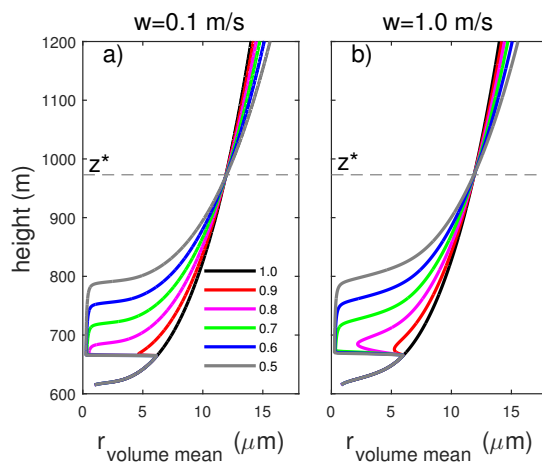


Figure 5. Volume-mean radius for a polydisperse cloud droplet population versus height at updraft speeds of a) $w = 0.1 \text{ m s}^{-1}$ and b) $w = 1.0 \text{ m s}^{-1}$ and for a clean environment. Line colors represent different mixing fractions χ , as in Figures 1 and 2. The horizontal dashed line is the critical height z^* predicted for a monodisperse cloud droplet population with equal volume-mean radius.

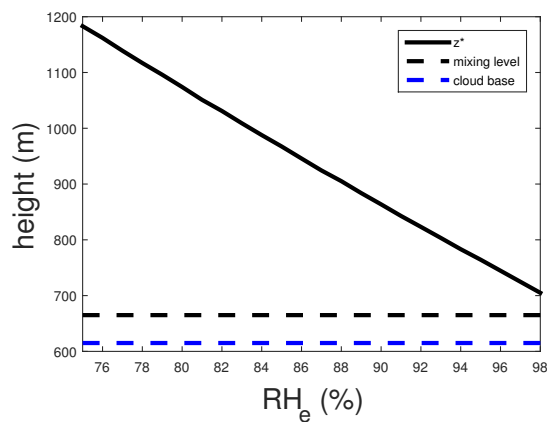


Figure 6. Critical height z^* versus environmental relative humidity RH_e at the mixing level. The height of cloud base (blue dashed line) and the mixing level (black dashed line) are shown for reference.